

Preparation of semiconductor nanospheres by laser-induced phase separation

Wen-Jing Qin,¹ Sergei A. Kulinich,² Xiao-Bo Yang,¹ Jing Sun,¹ and Xi-Wen Du^{1,a)}

¹*School of Materials Science and Engineering, Tianjin University, Tianjin, 300072, People's Republic of China*

²*Department of Applied Sciences, University of Quebec, Saguenay, PQ G7H 2B1, Canada*

(Received 22 July 2009; accepted 31 October 2009; published online 11 December 2009)

Semiconductor nanospheres were efficiently synthesized by the pulsed-laser-ablation-in-liquid technique applied to suspensions of certain powders. The nanosphere formation is demonstrated to follow a solid phase separation mechanism and take place in a low-temperature zone of the laser-irradiated volume, while the high temperature and rapid cooling rate generated by pulsed laser are crucial for the particle shape. The synthetic route is applied to different material systems and proved to be a general way for manufacturing various high-quality nanostructures with spherical shape. © 2009 American Institute of Physics. [doi:10.1063/1.3267298]

I. INTRODUCTION

Physical and chemical properties of nanostructures are well known to be closely related to their size and shape, and many fields would benefit from advances in the synthesis of well-defined nanostructures.^{1,2} Among various nanostructures, nanospheres have attracted much attention due to their remarkable properties and practical applications.^{3–5} For example, the hardness of silicon nanospheres was proved to be four times greater than that of bulk silicon;⁶ spherical colloids can serve as building blocks for photonic crystals owing to their low light scattering and high packing densities;^{7,8} spherical magnetic particles with slippery surface are prerequisite to high performance in function-specific biological applications.⁹

Up to now, many synthetic methods have been developed to prepare nanospheres, among which the two most commonly used are the glycol refluxing method and the hydrothermal (or solvothermal) method. Successful synthesis of nanospheres has been achieved in many material systems including pure metals, alloys, and chalcogenides.^{7,10–13} Nevertheless, the preparation of inorganic semiconductor nanospheres still remains a big challenge,^{14,15} the main obstacles are their high melting temperature and intense anisotropic growth of different crystal planes, especially on small-sized particles.¹⁶ Hence, obtaining semiconductor nanospheres smaller than 100 nm has been seldom reported in the literatures.^{17–19}

At high temperatures (HTs) close to the melting point, since the surface energy anisotropy is negligible,^{20,21} the equilibrium morphology of crystals must be close to sphere. As the temperature decreases, the surface anisotropy increases, and the equilibrium shape transforms into regular polyhedron, which is reached through surface diffusion.^{20,21} However, if the cooling rate is large enough, so that the surface diffusion is completely suppressed, the spherical shape is believed to be retained even at room temperature.

Pulsed laser ablation in liquid (PLAL) is a nonequilibrium process²² that can generate HTs necessary for the initial formation of spherical nanocrystals, as well as high cooling rates for quenching such nanostructures and preserving their shape.^{23,24} On the other hand, phase separation is well known to produce nanocrystals through the decomposition of unstable precursors, for example, silicon nanocrystals via the reaction $2\text{SiO} \rightarrow \text{Si} + \text{SiO}_2$.²⁵ Therefore, in the present work, we combine the PLAL technique with phase separation to synthesize semiconductor nanospheres. First, we conduct a thorough study on the laser-induced Si nanosphere formation mechanism. The results reveal that the Si nanospheres form in solid SiO matrix at temperatures close to the melting point of silicon. We then expand this synthetic route to one more material system and prepare SiC nanospheres. We thus demonstrate that the phase separation under extreme conditions created by the PLAL is a general way for synthesizing spherical nanocrystals in various material systems.

II. EXPERIMENT

Commercial SiO powder from Beijing Xmengtai Inc. (purity 99.99%), Si powder obtained by grinding a Si wafer, and SiOC powder obtained via a controlled pyrolysis process²⁶ were used as starting materials, all being ~200 mesh in size. An Nd: yttrium aluminum garnet pulsed laser was employed to irradiate the suspension (0.2 g of powder in 3 ml of liquid) in a glass cuvette for 10 min at room temperature. The laser wavelength, frequency, and pulse width were 1064 nm, 20 Hz, and 1.2 ms, respectively. The laser beam with power density of 12.3×10^6 W/cm² was focused about 5 mm below the liquid (normally de-ionized water) surface with a spot size of ~0.2 mm.

For comparison, a rapid thermal processor (RAPID-500) was employed to irradiate with an infrared lamp a similar SiO powder placed on a Si wafer. The powder was heated up to 1200 °C from room temperature during 5 s and kept at 1200 °C for 60 s, after which cooled down to room temperature also during 5 s. The basic experimental details for all samples are listed in Table I.

^{a)}Author to whom correspondence should be addressed. Tel.: +86 22 81523700. FAX: +86 22 27406796. Electronic mail: xwdu@tju.edu.cn.

TABLE I. Experimental conditions.

| Sample | Target | Liquid medium | Heating method | Time | Magnetic stirring |
|--------|--------|-------------------------------|----------------|--------|-------------------|
| A | SiO | H ₂ O | PLAL | 10 min | Yes |
| B | SiO | H ₂ O | PLAL | 10 min | No |
| C | Si | H ₂ O ₂ | PLAL | 10 min | Yes |
| D | SiO | N ₂ H ₄ | PLAL | 10 min | Yes |
| E | SiO | N/A | RTA | 60 s | N/A |
| F | SiOC | H ₂ O | PLAL | 10 min | Yes |

For more convenient observation, the products were etched in a HF solution (35.35 wt %, 1 ml) for 12 h to remove silicon oxides. The product morphology and structure were determined by scanning electron microscopy (SEM, Hitachi S-4800) and transmission electron microscopy (TEM, FEI Technai G2 F20) equipped with a field emission gun, and the composition was analyzed by energy-dispersive x-ray spectroscopy (Oxford INCA) attached to the TEM instrument. The phase composition was determined by using x-ray diffractometry (Rigaku D/max 2500v/pc). Magnetic property was detected at room temperature in a physical property measurement system (Quantum Design Co. USA).

III. RESULTS AND DISCUSSION

Sample A (see Table I for sample description) was prepared by irradiating a SiO suspension in de-ionized (DI) water under vigorous magnetic stirring. Figures 1(a) and 1(c) show SEM and high resolution TEM (HRTEM) images of the sample after HF etching and centrifugation. The images clearly prove that the agglomerated Si nanoparticles observed in the product possess a spherical shape. The x-ray diffraction (XRD) pattern [Fig. 1(b)] of the sample matches well with the data of diamondlike Si,⁴³ and its peaks can be indexed as (111), (220), and (311). The broad peaks arise from the glass matrix used to support the sample powder. Figure 1(d) shows some irregularly shaped nanocrystals that were also found, in small quantities, in this sample. These nanocrystals are much smaller but also well crystallized with

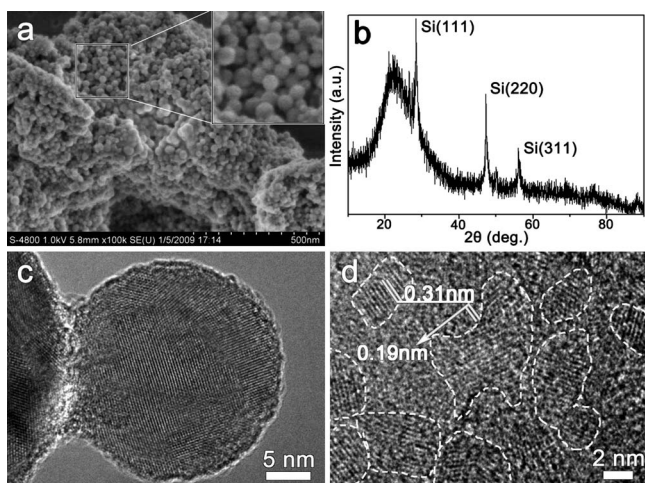


FIG. 1. Morphology and structure of products of PLAL-treated SiO suspension in water. (a) SEM image of nanospheres in sample A. (b) XRD pattern of the as-prepared sample. (c) HRTEM image of a Si nanosphere in sample A. (d) HRTEM image of irregularly shaped nanocrystals in sample A.

the observed interplanar distances of 0.31 and 0.19 nm, which coincide with the {111} and {220} spacings of diamondlike Si, respectively.²⁷

Sample B was prepared under the same conditions but without agitation of the liquid during laser treatment. As a result, the nanospheres in Fig. 2(b) are less homogeneous in size and roughly an order of magnitude bigger than those in sample A [Fig. 2(a)]. Irregular Si nanocrystals, similar to those in Fig. 1(d), were not found in sample B.

A suspension of Si powder in 30% H₂O₂ was also irradiated by pulsed laser under the same conditions as sample A. As seen in Fig. 2(c), only numerous irregularly shaped nanoparticles were observed in sample C. According to TEM analysis, they are well crystallized and, similar to those in Fig. 1(d), demonstrate interplanar distances of 0.31 and 0.19 nm, which correspond to Si {111} and {220} atomic planes, respectively.

Sample D was prepared by irradiating a SiO suspension in hydrazine hydrate (N₂H₄, 80%), all the other experimental conditions being the same as for sample A. As seen in Fig. 2(d), nanospheres could also be synthesized in this system, although the liquid medium was highly reductive. In addition, there was also another phase widely presented in this sample, which is amorphous according to the HRTEM image [inset in Fig. 2(d)] and selected area electron diffraction (SAED) pattern [Fig. 3(a)], while its energy-dispersive x-ray spectroscopy (EDS) results [Fig. 3(b)] showed mainly Si with a very small amount of oxygen.

A rapid thermal annealing (RTA) experiment, in which

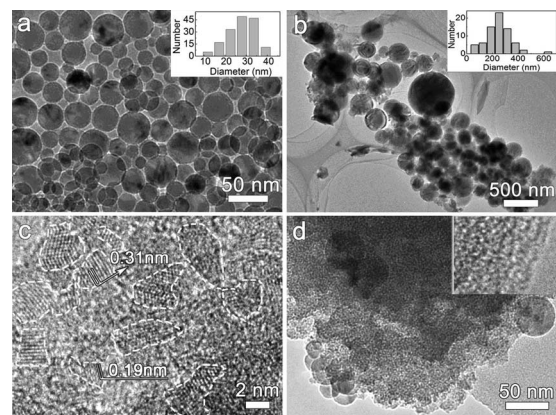


FIG. 2. Morphology of PLAL products prepared under different synthetic conditions. [(a) and (b)] Comparison of Si nanospheres in sample A and nonagitated sample B, respectively, the insets showing their size distribution. (c) HRTEM image of irregular nanocrystals in sample C. (d) TEM image of nanospheres and amorphous phase in sample D, the inset showing a HRTEM image of the amorphous phase.

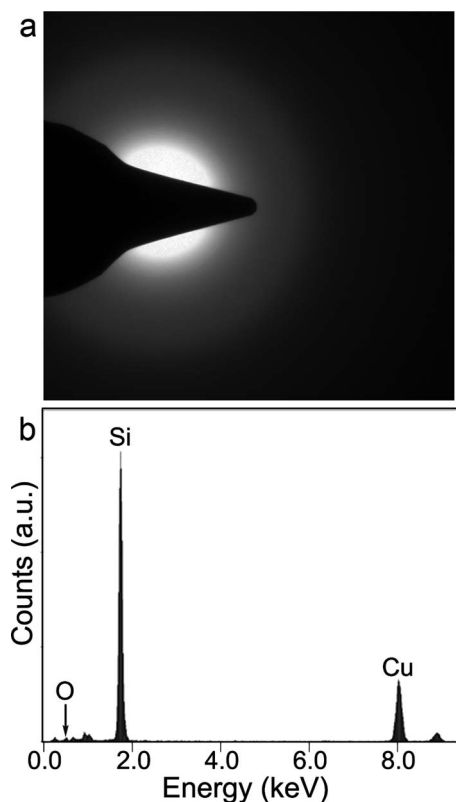


FIG. 3. Structure and composition of sample D. (a) Typical SAED pattern, (b) EDS spectrum of the amorphous phase in sample D, the Cu signal is from a Cu grid used to support sample during TEM observation.

high quenching rates were also reached, was carried out to compare its results with those of the PLAL technique. Nanocrystals with average size of 20 nm were found in sample E after 60 s of heat treatment at 1200 °C and relatively slow cooling down (to room temperature) during 5 s [Fig. 4(a)].

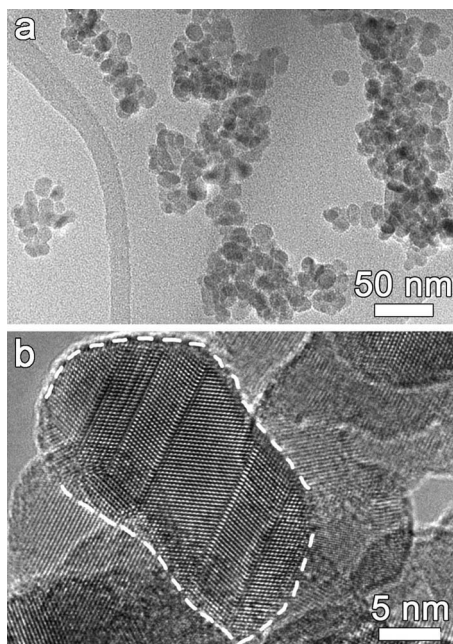


FIG. 4. Morphology of nanocrystals with facets in sample E prepared via RTA. (a) Low magnification TEM image, (b) HRTEM image, dashed line marks a nanocrystal with facets.

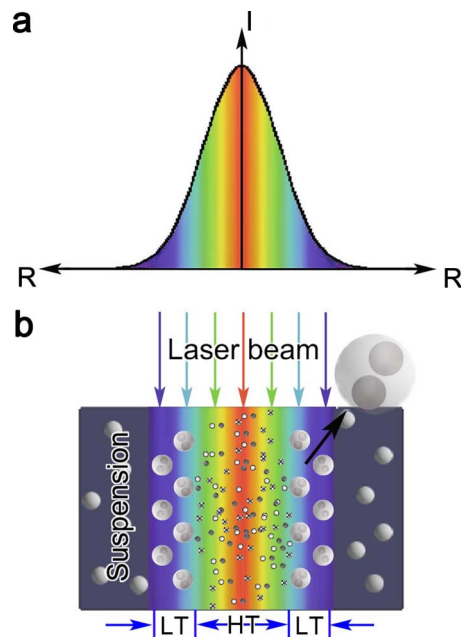


FIG. 5. (Color online) Schematic representation of intensity distribution in laser beam and corresponding temperature distribution in irradiated suspension. (a) Intensity distribution of laser beam, I and R standing for beam intensity and radius, respectively. (b) Temperature zones with different nanostructures obtained.

Noticeably, the morphology of the nanocrystals is not perfect sphere any longer, and facets are often seen at their edge [Fig. 4(b)].

To discuss the formation mechanism of the nanospheres, first we briefly mention the impact of laser beam on powder particles in liquid. It is well known that the laser beam possesses a Gaussian-like intensity distribution across its diameter, as schematically presented in Fig. 5(a). This results in a big temperature gradient inside the irradiated volume.²⁸ Since the pure liquid state of SiO only exists in a relatively narrow temperature range of 1725–1861 °C,²⁹ the solid and vapor phases are the two most likely expected when SiO particles are rapidly heated by the laser beam. Correspondingly, two temperature zones can be distinguished based on the phase state of SiO [Fig. 5(b)]. In the HT zone, temperatures are over the boiling point of the powder particles, and thus the particles can be vaporized or even turn to plasma state.^{30,31} The subsequent cooling of the vapor was reported to lead to coagulation and, often, formation of nanoparticles.³² Thus, the *evaporation-coagulation* processes are expected to prevail in the HT zone. In the low-temperature (LT) zone, temperatures are lower than the melting point of the target material (SiO). Therefore, the *solid phase separation* or *phase transformation* are the most conceivable processes there.^{33,34} The most significant difference between the evaporation-coagulation and phase transformation processes is that the former is influenced by the surrounding environment, such as pH value of the medium,³⁵ or the presence of surfactant,³⁶ whereas the latter is not.

The above described results suggest that the formation of the nanospheres takes place in the LT zone and follows the solid phase separation mechanism. The first evidence arises from the larger size of the spheres in sample B compared to

sample A. With no external agitation applied, the suspension in sample B stayed motionless, which allowed some SiO particles to be irradiated by numerous laser pulses, although the Brownian motion and/or convection could eventually move them out of the irradiated zone. In the HT zone, SiO particles (and possibly some products of SiO decomposition from the LT zone) are vaporized and coagulate as Si nanocrystals after each pulse, and the as-formed Si nanocrystals and water pass through the evaporation-coagulation process repeatedly during the following laser pulses. The final size of the Si nanocrystals can eventually decrease down to zero due to oxidization by water vapor during repeating coagulation cycles, if they remain in the HT zone. Thus, the Si nanospheres are very unlikely to grow bigger under longer irradiation in this zone. Meanwhile, in the LT zone, SiO particles can be heated to generate silicon nanocrystals via solid phase separation mechanisms, and such Si cores can grow up continuously inside the SiO particles during the following pulses because the solid SiO matrix can supply Si atoms via its decomposition. This provides the continuous growth and prevents the silicon cores from oxidization by the liquid medium. Hence, the observed larger nanospheres in sample B definitely support the solid phase separation mechanism and nanosphere formation in the LT zone.

We further prove the sphere formation through the solid phase separation by excluding the evaporation-coagulation mechanism. Sample C was designed to simulate the evaporation-coagulation processes by using a Si powder as a starting material, since it does not allow for any phase separation, and the evaporation-coagulation processes are the only route to generate new products in this system. To compensate for oxygen, released during SiO decomposition, we used H₂O₂ in this sample. Hence, the Si–H₂O₂ system used in sample C could simulate the processes that the SiO–H₂O system (sample A) undergoes in the HT zone, whereas it could not provide any phase separation processes expected in the LT zone of sample A. The results indicate that the evaporation-coagulation processes (which were expected to result in similar products in samples A and C) can only produce the irregular Si nanocrystals [shown in Figs. 1(d) and 2(c)] rather than nanospheres. In other words, the nanospheres are only produced by the solid-phase-separation processes taking place in the LT zone.

Sample D provides more support to the solid phase separation mechanism through the replacement of the liquid medium. The liquid media in samples A and D differed significantly in redox properties. Nevertheless, as shown in Figs. 2(a) and 2(d), the nanospheres were synthesized in both systems (SiO–H₂O and SiO–N₂H₄). At the same time, the by-product in these systems appears to be strongly influenced by the redox properties of the liquid medium. In the more oxidizing medium [sample A, Fig. 1(d)], the by-product is irregularly-shaped Si nanocrystals incorporated into amorphous Si matrix, while in the more reductive medium, the by-product is amorphous silicon [inset of Fig. 2(d)], and its amount is much larger than that in sample A. This finding suggests the by-product is generated via the evaporation-coagulation processes which can be significantly affected by the liquid medium. The oxidizing medium (H₂O) in sample

A could be vaporized and react with silicon in the HT zone, giving rise mainly to silicon oxide and leaving only a small amount of Si atoms, which appeared to coagulate and, partially, crystallize as irregularly shaped nanocrystals well seen in Fig. 1(d). In contrast, the reductive medium (N₂H₄) in sample D was expected to react, during quenching, with oxygen (from SiO decomposition) in the HT zone, producing water and a large amount of silicon. Due to the high cooling rates provided by the PLAL, such Si atoms were quenched by the liquid and coagulated as amorphous phase which is well observed in Fig. 2(d).

Next, we discuss the decisive factors for the spherical shape of the nanocrystals. The growth time (1 min) for the nanocrystals in sample E prepared through the RTA method was significantly longer than that for the nanospheres in sample A, where a pulse period was $\sim 1/20$ s, and each SiO particle was likely to be irradiated by a single laser pulse due to vigorous stirring. However, the nanocrystals in sample E are smaller than those in sample A [Figs. 4(a) and 2(a)], thus implying much higher growth rates in the PLAL process.

Silicon nanocrystals produced by phase separation of SiO are known to follow a diffusion-controlled growth, in which the growth rate can be described as³⁷

$$\left(\frac{dr}{dt}\right)_{r_i} = \frac{D_0 \exp(-Q/RT)}{C^b - C^a} \left(\frac{\partial C}{\partial r}\right)_{r_i},$$

where r_i is the initial silicon cluster radius, D_0 is the prefactor of the diffusion coefficient of Si in SiO₂, C^a is the composition of stoichiometric SiO₂, C^b is the composition of silicon cluster, and C is the composition in the oxide matrix near the silicon cluster, Q is the activation energy of Si diffusion and R is the universal gas constant, and T is the absolute temperature. For a given SiO_x system, all the parameters are constant except for the temperature.

The above formula indicates that high growth rates of Si nanocrystals in SiO matrix are associated with high temperatures. Therefore, we can deduce that the nanospheres in the PLAL experiments grew up at higher temperatures than that in the RTA experiment (1200 °C). The growth temperatures were thus close to the melting point of crystal bulk Si (1412 °C), where its nanoparticles are believed to have very small surface anisotropy and form as spheres. After the withdrawal of a laser pulse, the hot (spherical) particles were immediately exposed to a cool liquid medium, with a huge temperature difference causing very high cooling rates. As a result, the Si nanospheres in their matrix particles were quenched, and their perfect round shape was thus maintained intact down to room temperature. In contrast, the cooling rate in the RTA was much lower than those in the PLAL. Therefore, the surface diffusion could still proceed during the cooling stage, which led to irregular shape of the particles in Fig. 4, with many facets approximate to the equilibrium shape at room temperature.

We measured the magnetic property of silicon nanospheres at different temperatures, as shown in Fig. 6. The sample exhibits diamagnetic and ferromagnetic features at room temperature (300 K), but paramagnetic property at LT (5 K). The unusual ferromagnetic property has been recently

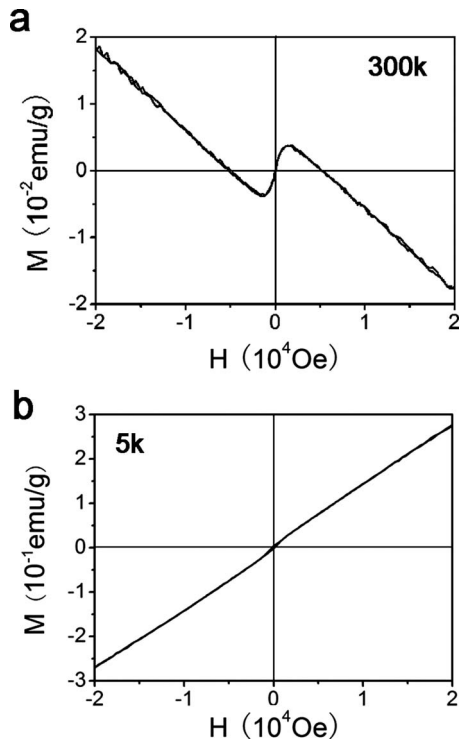


FIG. 6. Magnetic properties of the sample containing silicon nanospheres, (a) at 300 K and (b) at 5 K.

found in etched silicon, and was attributed to the contamination by iron metal;^{38,39} however, iron element has not been found in our product [see Fig. 3(b)]. We propose that the ferromagnetic signals may arise from both quantum size effects and the magnetic coupling between nanospheres, similar to the case in the germanium quantum dots.⁴⁰ The paramagnetic property at LT may be caused by the defects in silicon nanospheres or the surface atoms of silicon contain unpaired electrons.⁴¹ Nevertheless, the precise mechanism is not yet known, and need further investigation.

The above discussion demonstrates that the PLAL technique possesses the unique capability of preparing regularly shaped nanospheres by treating materials prone to solid phase separation. Below, we further expand this method and apply it to the SiOC system, producing SiC spheres via the phase separation. Amorphous SiOC is well known to be separated into SiC, SiO₂ and C under heat treatment.⁴² Therefore, to prepare sample F, we treated a suspension of SiOC powder in DI water, applying the same process conditions as those for the Si nanospheres (see Table I).

The starting SiOC powder was predominately amorphous according to the HRTEM image [Fig. 7(a)] and XRD pattern [Fig. 7(c)]. After laser ablation of its suspension in DI water and etching in HF acid, the sample demonstrates a diversiform appearance, where numerous crystalline particles with round shape are embedded in a network matrix, as seen in the TEM image in Fig. 7(b). The XRD patterns in Fig. 7(c) confirm the transformation from amorphous to crystalline during the laser irradiation of the SiOC suspension. The structure of the crystal phase matches well the fcc structure of SiC,⁴⁴ as the new arisen peaks in Fig. 5(b) can be indexed as (111), (200), (220), and (311). The EDS spectra in Fig.

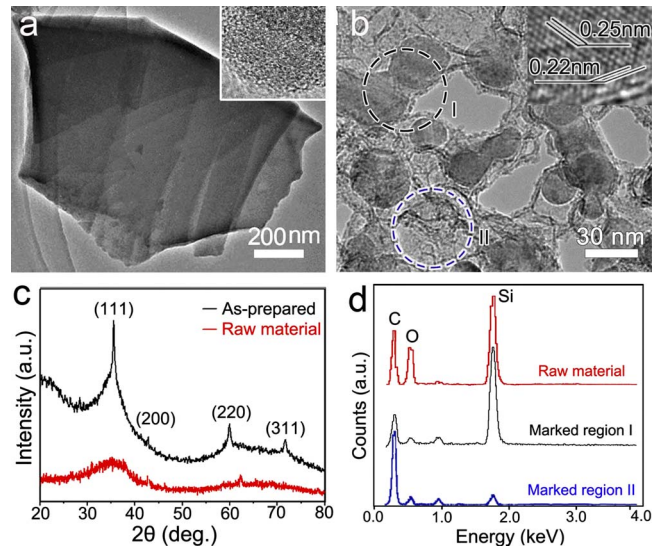


FIG. 7. (Color online) The raw SiOC material and product of PLAL-treated SiOC suspension in water. (a) TEM image of amorphous SiOC powder. The inset shows a HRTEM image. (b) TEM image of SiC nanospheres with carbon network in sample F after HF etching, (c) XRD patterns of raw SiOC and sample F, and (d) EDS spectra (probe size 40 nm) of raw SiOC and etched sample F taken over the two regions marked in (b).

7(d) show that the nanocrystals are mainly composed of silicon and carbon, while the surrounding matrix is based on carbon. The small Si signal, also detected in the matrix region (II), is likely to arise from fine SiC clusters embedded into the carbon network.

The round nanoparticles in Fig. 7(b) are single crystals with the interplanar distances observed to be ~ 0.25 and ~ 0.22 nm [Fig. 7(b), inset], which is consistent with the interplanar distances for SiC {111} and {200} planes, respectively. Thus the combination of XRD and HRTEM analyses allows to conclude the particles under consideration are SiC nanocrystals, which agrees well with the EDS spectrum (from region I) in Fig. 7(d). The above results strongly support the PLAL-induced solid phase separation as a general and effective way toward various nanospheres with regular geometry. And thus other sphere-shaped nanomaterials are likely to be prepared by this technique in the future.

IV. CONCLUSIONS

We carry out a detailed analysis of the new approach for the large-scale preparation of nanospheres. The technique combines the PLAL with solid phase separation of a target material. The growth mechanism for Si nanospheres prepared through this method is proved to be a typical solid state phase separation in a lower-temperature zone of the laser-irradiated suspension of SiO in liquid, while the high temperatures and rapid cooling rates generated by pulsed laser are crucial for the formation and quenching of the nanospheres. Following the same procedure, SiC nanospheres have been synthesized by irradiating an amorphous SiOC powder suspension in DI water under magnetic stirring. Combining the advantages of conventional phase separation and laser ablation with low instrumental temperatures and inexpensive precursors, while being a much more straightforward and rapid process, the laser-induced phase separation

appears to be a very promising technique for preparing spherical nanoparticles, which can be expanded to other material systems.

ACKNOWLEDGMENTS

This work was supported by the Natural Science Foundation of China (Grant Nos. 10732020 and 50672065) and Chinese 863 project 2007AA021808 and 2009AA03Z301.

- ¹Y. W. Jun, J. S. Choi, and J. Cheon, *Angew. Chem., Int. Ed.* **45**, 3414 (2006).
- ²C. Burda, X. B. Chen, R. Narayanan, and M. A. El-Sayed, *Chem. Rev. (Washington, D.C.)* **105**, 1025 (2005).
- ³J. D. Joannopoulos, P. R. Villeneuve, and S. Fan, *Nature (London)* **386**, 143 (1997).
- ⁴F. Caruso, R. A. Caruso, and H. Mohwald, *Science* **282**, 1111 (1998).
- ⁵D. J. Norris and Y. A. Vlasov, *Adv. Mater.* **13**, 371 (2001).
- ⁶W. W. Gerberich, W. M. Mook, C. R. Perrey, C. B. Carter, M. I. Baskes, R. Mukherjee, A. Gidwani, J. Heberlein, P. H. McMurry, and S. L. Girshick, *J. Mech. Phys. Solids* **51**, 979 (2003).
- ⁷X. C. Jiang, T. Herricks, and Y. N. Xia, *Adv. Mater.* **15**, 1205 (2003).
- ⁸U. Jeong, Y. L. Wang, M. Ibsate, and Y. N. Xia, *Adv. Funct. Mater.* **15**, 1907 (2005).
- ⁹H. Deng, X. L. Li, Q. Peng, X. Wang, J. P. Chen, and Y. D. Li, *Angew. Chem., Int. Ed.* **44**, 2782 (2005).
- ¹⁰U. Jeong and Y. N. Xia, *Adv. Mater.* **17**, 102 (2005).
- ¹¹Y. L. Wang and Y. N. Xia, *Nano Lett.* **4**, 2047 (2004).
- ¹²J. T. Zhang, J. F. Liu, Q. Peng, X. Wang, and Y. D. Li, *Chem. Mater.* **18**, 867 (2006).
- ¹³P. Y. Song, J. F. Wang, C. P. Chen, H. Deng, and Y. D. Li, *J. Appl. Phys.* **100**, 044314 (2006).
- ¹⁴F. Wang, G. Y. Xu, Z. Q. Zhang, and X. Xin, *Eur. J. Inorg. Chem.* **2006**, 109 (2006).
- ¹⁵Y. Zhang and Y. D. Li, *J. Phys. Chem. B* **108**, 17805 (2004).
- ¹⁶A. Yurtsever, M. Weyland, and D. A. Muller, *Appl. Phys. Lett.* **89**, 151920 (2006).
- ¹⁷H. G. Yang and H. C. Zeng, *J. Phys. Chem. B* **108**, 3492 (2004).
- ¹⁸Y. Z. Zhang, Y. P. Liu, L. H. Wua, H. Lia, L. Z. Han, B. C. Wang, and E. Q. Xie, *Appl. Surf. Sci.* **255**, 4801 (2009).
- ¹⁹K. P. Velikov and A. V. Blaaderen, *Langmuir* **17**, 4779 (2001).
- ²⁰C. R. Henry, *Prog. Surf. Sci.* **80**, 92 (2005).
- ²¹J. J. Metois and J. C. Heyraud, *Ultramicroscopy* **31**, 73 (1989).
- ²²G. W. Yang, *Prog. Mater. Sci.* **52**, 648 (2007).
- ²³K. Fukutani, *Adv. Mater.* **16**, 1456 (2004).
- ²⁴J. Sun, S. L. Hu, X. W. Du, Y. W. Lei, and L. Jiang, *Appl. Phys. Lett.* **89**, 183115 (2006).
- ²⁵J. Qiu, W. Q. Shen, R. J. Yu, and B. D. Yao, *Chem. Lett.* **37**, 644 (2008).
- ²⁶E. Radovanovic, M. F. Gozzi, M. C. Goncalves, and I. V. P. Yoshida, *J. Non-Cryst. Solids* **248**, 37 (1999).
- ²⁷W. S. Shi, H. Y. Peng, Y. F. Zheng, N. Wang, N. G. Shang, Z. W. Pan, C. S. Lee, and S. T. Lee, *Adv. Mater.* **12**, 1343 (2000).
- ²⁸C. Fauteux, R. Longtin, J. Pegna, and D. Therriault, *Inorg. Chem.* **46**, 11036 (2007).
- ²⁹H. Okamoto, *J. Phase Equilib. Diffus.* **28**, 309 (2007).
- ³⁰T. Makimura, T. Mizuta, T. Takahashi, and K. Murakami, *Appl. Phys. A: Mater. Sci. Process.* **79**, 819 (2004).
- ³¹D. B. Geohegan, A. A. Puzos, G. Duscher, and S. J. Pennycook, *Appl. Phys. Lett.* **72**, 2987 (1998).
- ³²C. X. Wang, P. Liu, H. Cui, and G. W. Yang, *Appl. Phys. Lett.* **87**, 201913 (2005).
- ³³A. Takami, H. Kurita, and S. Koda, *J. Phys. Chem. B* **103**, 1226 (1999).
- ³⁴F. Vidal, T. W. Johnston, S. Laville, O. Barthelemy, M. Chaker, B. Le Droff, J. Margot, and M. Sabsabi, *Phys. Rev. Lett.* **86**, 2573 (2001).
- ³⁵C. He, T. Sasaki, H. Usui, Y. Shimizu, and N. Koshizaki, *J. Photochem. Photobiol., A* **191**, 66 (2007).
- ³⁶T. Tsuji, D. H. Thang, Y. Okazaki, M. Nakanishi, Y. Tsuboi, and M. Tsuji, *Appl. Surf. Sci.* **254**, 5224 (2008).
- ³⁷L. A. Nesbit, *Appl. Phys. Lett.* **46**, 38 (1985).
- ³⁸P. J. Grace, M. Venkatesan, J. Alaria, J. Michael, D. Coey, G. Kopnov, and R. Naaman, *Adv. Mater.* **21**, 71 (2009).
- ³⁹G. Kopnov, Z. Vager, and R. Naaman, *Adv. Mater.* **19**, 925 (2007).
- ⁴⁰Y. Liou and Y. L. Shen, *Adv. Mater.* **20**, 779 (2008).
- ⁴¹A. Stesmans and V. V. Afanas'ev, *Phys. Rev. B* **57**, 10030 (1998).
- ⁴²G. T. Burns, R. B. Taylor, Y. R. Xu, A. Zangvil, and G. A. Zank, *Chem. Mater.* **4**, 1313 (1992).
- ⁴³JCPDS Card No. 27-1402.
- ⁴⁴JCPDS Card No. 65-0360.